

Gas-rich Ultra-diffuse Galaxies Are Originated from High Specific Angular Momentum

YU RONG,¹ HUIJIE HU,^{2,3} MIN HE,³ WEI DU,³ QI GUO,³ HUI-YUAN WANG,¹ HONG-XIN ZHANG,¹ AND HOJUN MO⁴

¹*Department of Astronomy, University of Science and Technology of China, Hefei, Anhui 230026, China*

²*University of Chinese Academy of Sciences, Beijing 100049, China*

³*National Astronomical Observatories, Chinese Academy of Sciences, Beijing 100012, China*

⁴*Department of Astronomy, University of Massachusetts Amherst, MA 01003, USA*

(Received April 2, 2024; Revised tomorrow; Accepted the day after tomorrow)

Submitted to ApJ

ABSTRACT

Ultra-diffuse galaxies, characterized by comparable effective radii to the Milky Way but possessing 100-1,000 times fewer stars, offer a unique opportunity to garner novel insights into the mechanisms governing galaxy formation. Nevertheless, the existing corpus of observational and simulation studies has not yet yielded a definitive constraint or comprehensive consensus on the formation mechanisms underlying ultra-diffuse galaxies. In this study, we delve into the properties of ultra-diffuse galaxies enriched with neutral hydrogen using a semi-analytic method, with the explicit aim of constraining existing ultra-diffuse galaxy formation models. We find that the gas-rich ultra-diffuse galaxies are statistically not failed L^* galaxies nor dark matter deficient galaxies. In statistical terms, these ultra-diffuse galaxies exhibit comparable halo concentration, but higher baryonic mass fraction, as well as higher stellar and gas specific angular momentum, in comparison to typical dwarf galaxy counterparts. Our analysis unveils that higher gas specific angular momentum serves as the underlying factor elucidating the observed heightened baryonic mass fractions, diminished star formation efficiency, expanded stellar disk sizes, and reduced stellar densities in ultra-diffuse galaxies. Our findings make significant contributions to advancing our knowledge of ultra-diffuse galaxy formation and shed light on the intricate interplay between gas dynamics and the evolution of galaxies.

Keywords: galaxies: dwarf — galaxies: photometry — galaxies: evolution — methods: statistical

1. INTRODUCTION

Ultra-diffuse galaxies (UDGs) (van Dokkum et al. 2015) epitomize a distinctive category of galactic entities distinguished by stellar masses akin to those of traditional dwarf galaxies, yet manifesting effective radii akin to that of the Milky Way. They currently occupy a pivotal position in the domain of galactic inquiry. UDGs are characterized by their exceedingly low surface brightness and an extensive stellar disk structure, resulting in a marked deviation in their distribution on the stellar mass versus effective radius plot compared to typical dwarf and massive galaxies (van Dokkum et al. 2015; Leisman et al. 2017; Rong et al. 2020a). Within the framework of the Lambda Cold Dark Matter (ΛCDM) paradigm, prevailing galaxy evolution models generally presuppose a relatively uniform correlation between a galaxy’s stellar mass and its effective radius (Guo et al. 2011). Conse-

quently, the distinctive distribution of UDGs implies a potential substantial disparity in their formation mechanism compared to typical galaxies, thus positioning UDGs as a unique vantage point for scrutinizing established galaxy evolution models and comprehending the galaxy formation process. While multiple theoretical models have been posited to elucidate the genesis of UDGs (Rong et al. 2017; Di Cintio et al. 2017; Carleton et al. 2019; Wright et al. 2021; Grishin et al. 2021), a consensus remains elusive.

UDGs are widespread across galaxy clusters, groups, and low-density environments. Those located in high-density regions, such as galaxy clusters, are likely enveloped by substantial dark matter halos, suggesting that UDGs in dense locales may represent “failed” L^* galaxies (FLG) (van Dokkum et al. 2015), with dark matter halo masses commensurate to that of the Milky Way, despite their stellar masses resembling typical dwarf galaxies. Notably, the largest UDG in the Coma cluster, DF44, has been ascertained (van Dokkum et al. 2016) to harbor a dark matter halo mass of $10^{12} M_{\odot}$. However, subsequent statistical analyses of UDG samples, encompassing the number/mass of globular clusters and weak lensing,

indicate that the majority of UDGs in galaxy clusters possess masses akin to typical dwarf galaxies ($\sim 10^{11} M_\odot$), markedly diverging from the mass of the Milky Way (Sifón et al. 2018; Peng & Lim 2016). Additionally, investigations into the dynamics of globular clusters in two UDGs (DF2 and DF4) within the NGC 1052 galaxy group suggest that these UDGs exhibit minimal dark matter ($\lesssim 10^7 M_\odot$) (van Dokkum et al. 2018, 2019a), indicating that certain UDGs may even represent dark matter-deficient dwarf galaxies (DMDD). The wide range of masses spanning from FLG to DMDD underscores the significant divergence in the formation and evolution of UDGs from typical galaxies, potentially challenging established galaxy evolution models.

Returning to the question of the formation mechanism of UDGs, theoretically, disregarding the gravitational influence of baryonic matter, we can express the scale length and central surface density of the stellar disk formed at the core of a dark matter halo as follows (Mo et al. 1998),

$$R_{*,d} = \frac{J_*}{2M_*V_c} = \frac{S_*}{2V_c} \quad (1)$$

$$\Sigma_{*,0} = \frac{J_*}{4\pi V_c R_{*,d}^3} = \frac{2M_*V_c^2}{\pi S_*^2} \quad (2)$$

Here, V_c represents the circular velocity of the halo, and M_* , J_* , as well as $S_* \equiv J_*/M_*$ characterize the mass, angular momentum, and specific angular momentum of the stellar disk, respectively. Therefore, the extended stellar distribution and low surface brightness observed in UDGs can potentially be elucidated through the following three conjectures:

(I). **Higher S_* :** Previous cosmological hydrodynamical simulations (Benavides et al. 2023; Liao et al. 2019) and N -body simulations employing semi-analytic galaxy formation models (Rong et al. 2017; Amorisco & Loeb 2016) lend support to a high-spin UDG formation scenario. These simulations posit that UDGs acquire augmented specific angular momenta from their high-spin halos. Another proposed model, involving the merging of dwarf galaxies (Wright et al. 2021), postulates the transient amplification of descendant halos' spin during merging events to reproduce UDGs. Alternatively, UDGs may have experienced the accretion of circumgalactic medium with elevated spins while maintaining a normal halo angular momentum J_h comparable to typical dwarf galaxies (Posti et al. 2018; Mancera Piña et al. 2020). This circumgalactic medium subsequently cools, fostering star formation and converting the heightened specific angular momentum into the stellar disk. Both scenarios, characterized by an increased halo spin and enhanced conversion efficiency $j_* \equiv J_*/J_h$, consistently yield greater specific angular momenta S_* for the stellar constituents within UDGs.

Several observational inquiries into the internal kinematics of UDGs have indicated that the specific angular momentum of their stellar disks may parallel that of typical dwarf galaxies, or even suggested the absence of significant rotational motion in UDGs (e.g. Chilingarian et al. 2019; van Dokkum et al. 2019b). Consequently, these findings have

led researchers to speculate that UDGs may not have originated from dark matter halos characterized by high spin, nor do they exhibit high-spin stellar disks. It is pertinent to note, however, that these observations have predominantly focused on UDGs in high-density environments, where these UDGs have already undergone tidal heating from massive galaxies (e.g., Rong et al. 2020b; Mancera Piña et al. 2019), potentially diminishing their original spin, even if it was initially substantial. Nevertheless, these observational inquiries do not preclude the possibility that UDGs in low-density regions may have emerged from higher spin.

Furthermore, certain hydrodynamic simulations (e.g., NIHAO and FIRE) have suggested that the spin of UDGs is akin to that of typical dwarf galaxies (e.g., Di Cintio et al. 2017; Chan et al. 2018; Cardona-Barrero et al. 2020). However, it is important to note that these simulations are not comprehensive cosmological simulations, but rather zoom-in simulations involving a limited number of samples, and as such, lack statistical significance. In contrast, comprehensive cosmological hydrodynamic simulations such as the IllustrisTNG have indeed demonstrated that the spin statistics of UDGs exceed those of typical dwarf galaxies (Benavides et al. 2023). Consequently, the hypothesis that high spin represents a plausible mechanism for the formation of UDGs, particularly in low-density regions, emerges as a compelling and potentially the most robust model of formation to date.

(II). **Elevated V_c and diminished M_* :** The failed L^* formation model (van Dokkum et al. 2015) for UDGs posits the coexistence of massive host halos on par with the Milky Way (resulting in an intensified V_c akin to that of the Milky Way, given the relationship $M_{\text{vir}} \propto V_c^3$; Mo et al. 1998), alongside reduced stellar masses resembling those of typical dwarf galaxies. This attenuation in stellar mass could potentially arise from the influences of tidal interactions or ram pressure effects during the nascent stages of the Universe (Yozin & Bekki 2015).

(III). **Change of gravitational potential:** Equations (1) and (2) hold true only if the gravitational effects of galactic baryonic matter and the environment can be neglected (Mo et al. 1998). In the cases of the outflow model (Chan et al. 2018; Di Cintio et al. 2017), tidal interaction model (Carleton et al. 2019; Rong et al. 2020b; Jiang et al. 2019), or environmental stripping model (Grishin et al. 2021) for UDG formation, the stellar orbits in UDGs expand due to significant changes in gravitational potentials.

We have systematically categorized the existing UDG formation models into these three possibilities. To ascertain the decisive factor among the aforementioned possibilities for UDG formation, in this investigation we adopt a rigorous semi-analytic approach and analyze the single-dish neutral hydrogen (HI) and optical photometric data from the Arecibo Legacy Fast Alfa Survey (ALFALFA $\alpha.100$) (Giovanelli et al. 2005; Haynes et al. 2018) and Twelfth Data Release of the Sloan Digital Sky Survey (SDSS DR12) (Alam et al. 2015) to scrutinize the baryonic fractions and kinematics of HI-bearing UDGs. In section 2, we introduce the UDG samples studied in this work. In section 3, we investigate and compare

the properties of gas-rich UDGs and typical dwarf counterparts, which imply the formation mechanism of UDGs. We discuss and summarize our results in section 4. In this paper, we use “log” to represent “ \log_{10} ”.

2. GAS-RICH UDGs IN OBSERVATION

2.1. Sample selection

The UDG sample is identified from the cross-matched catalog of ALFALFA and SDSS. For ALFALFA galaxies with optical counterparts, we meticulously employ the SEXTRACTOR software (Bertin & Arnouts 1996) to precisely measure the g and i -band ‘mag_auto’ magnitudes, effective radius $R_{*,e}$, as well as apparent axis ratio of each galaxy using the method proposed by Du et al. (2015) (Du et al. 2015). To derive the absolute magnitudes M_g and M_i for galaxies with varying axis ratios and colors, we adopt the methodology outlined in Durbala et al. (2020) (Durbala et al. 2020) to mitigate the influence of internal dust extinctions within the galaxies. Furthermore, we utilize the i -band absolute magnitudes M_i and $g - i$ colors to estimate galactic stellar masses M_* , employing the mass-to-light ratios $\log(M_*/L_i) = 0.70(g - i) - 0.68 - 0.057$ (Taylor et al. 2011), where -0.057 is a correction factor accounting for a Kroupa initial mass function (Kroupa 2002; Herrmann et al. 2016). Subsequently, we estimate the mean stellar surface density within the effective radius as $\langle \Sigma_* \rangle_e \simeq M_*/2\pi R_{*,e}^2$.

For the UDG selection, we adopt a criterion of $\langle \Sigma_* \rangle_e \leq 10^7 M_\odot/\text{kpc}^2$, in conjunction with $R_e > 1.5 \text{ kpc}$ and $M_* < 10^9 M_\odot$, as shown in Fig. 1. This selection criterion is slightly different from the conventional criterion of identifying UDGs, which relies on surface brightness, R_e , and M_* . This updated approach addresses the challenge posed by varying mass-to-light ratios among different UDGs and ensures a more unbiased selection of UDG samples, particularly for galaxies exhibiting abundant HI gas, ongoing star formation, and low stellar mass-to-light ratios. In contrast, the traditional approach tends to favor UDGs with redder colors. For the UDGs in galaxy clusters and groups, with a typical color of $g - r \sim 0.6$ (Rong et al. 2017) and corresponding r -band mass-to-light ratio of approximately $\log(M_*/L_*) \sim 0.202$ (Bell et al. 2003), $\langle \Sigma_* \rangle_e \leq 10^7 M_\odot/\text{kpc}^2$ corresponds to a surface brightness threshold of $\langle \mu_* \rangle_e \geq 24 \text{ mag/arcsec}^2$ in the r -band, which is consistent with the selection criterion used in the work of van Dokkum et al. (2015) and van der Burg et al. (2016).

To ensure the accuracy of UDG selection and avoid potential errors arising from internal dust extinctions, galaxies with optical apparent axis ratios $b/a < 0.2$ are excluded. UDGs with $b/a > 0.7$ or low HI signal-to-noise ratios ($\text{SNR} < 10$) are also eliminated due to significant uncertainties in estimating circular velocities. Additionally, UDGs with contaminated photometries, suspicious HI spectra, pronounced irregular optical images, or galaxy companions within a radial velocity difference $\Delta v < 500 \text{ km/s}$ and a projected radius $R_p < 7 \text{ arcmin}$ (twice the beam size of Arecibo) are excluded, as such companions could potentially interact with UDGs or

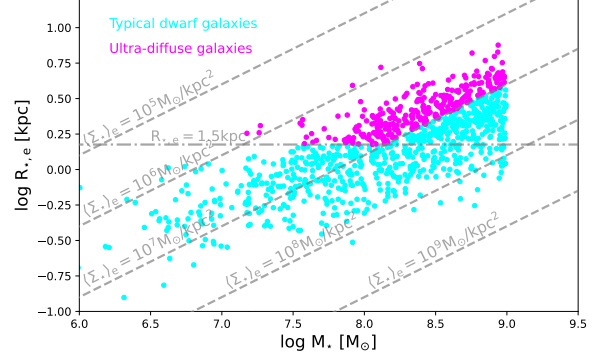


Figure 1. Stellar mass M_* vs. effective radius $R_{*,e}$ plot for UDGs (depicted by magenta circles) and typical dwarf counterparts (depicted by cyan circles).

introduce inaccuracies in estimating HI masses from the HI spectra.

Consequently, a sample of 321 UDGs is obtained. The stellar masses of our UDG sample range from approximately 10^7 to $10^9 M_\odot$. To ensure a fair comparison of UDG properties with typical dwarf galaxies, galaxies with $M_* \leq 10^9 M_\odot$ but $\langle \Sigma_* \rangle_e > 10^7 M_\odot/\text{kpc}^2$ or $R_{*,e} \leq 1.5 \text{ kpc}$ are selected as the sample of typical dwarf counterparts.

It is noteworthy that a subset of ALFALFA galaxies lacking optical counterparts or exhibiting exceedingly faint optical signatures, commonly referred to as “dark galaxies” (Disney 1976; Janowiecki et al. 2015), may fulfill the selection criteria based on effective radii and surface densities typically associated with UDGs. Nevertheless, multiple investigations have revealed that these dark galaxies are susceptible to tidal interactions (Román et al. 2021; Duc & Bournaud 2008), rendering them non-equilibrium systems. Consequently, our study excludes these entities due to the inherent challenge in accurately estimating their circular velocities and halo masses.

2.2. Circular velocity and halo mass estimation

In this study, we estimate the circular velocities V_c and halo masses M_{vir} for the selected UDGs and typical dwarf counterparts.

In the absence of resolved HI data, we employ the optical b/a ratio to estimate the HI disk inclination ϕ , using $\sin \phi = \sqrt{(1 - (b/a)^2)/(1 - q_0^2)}$, where $q_0 \sim 0.2$ (Tully et al. 2009; Giovanelli et al. 1997; Li et al. 2022) represents the intrinsic thickness of a galaxy. The circular velocity, $V_c = W_{20}/2/\sin \phi$ (W_{20} being the 20% peak width of the HI line after correction for instrumental broadening (Haynes et al. 2018; Guo et al. 2020; Hu et al. 2023)), is consequently computed. We note that W_{20} has been proved to be a good indicator of the asymmetric drift-corrected circular velocity using the kinematics maps of dwarf galaxies in the LITTLE THINGS (Hunter et al. 2012) by Guo et al. (2020).

We introduce the HI radius r_{HI} , which corresponds to the radius at which the HI surface density attains $1 M_\odot \text{pc}^{-2}$.

The estimation of r_{HI} is facilitated by the tight correlation observed between r_{HI} and HI mass M_{HI} , as inferred from empirical observations: $\log r_{\text{HI}} = 0.51 \log M_{\text{HI}} - 3.59$ (Wang et al. 2016; Gault et al. 2021).

We adopt the method proposed by Guo et al. (2020) to estimate the halo mass of each galaxy. Assuming a spherically symmetric dark matter halo model, we calculate the dynamical mass enclosed within the HI radius r_{HI} ,

$$M_{\text{dy}}(< r_{\text{HI}}) = V_c^2 r_{\text{HI}} / G, \quad (3)$$

where G represents the gravitational constant. The halo mass M_{vir} is then estimated by assuming a Burkert dark matter profile (Burkert 1995), and utilizing the equations,

$$\begin{aligned} M_{\text{dy}}(< r_{\text{HI}}) - M_{\text{bar}} &= \int_0^{r_{\text{HI}}} 4\pi r^2 \rho(r) dr \\ &= 2\pi \rho_0 R_0^3 \left[\ln\left(1 + \frac{r_{\text{HI}}}{R_0}\right) + 0.5 \ln\left(1 + \frac{r_{\text{HI}}^2}{R_0^2}\right) - \arctan\left(\frac{r_{\text{HI}}}{R_0}\right) \right], \end{aligned} \quad (4)$$

and

$$\begin{aligned} M_{\text{vir}} &= \int_0^{R_{\text{vir}}} 4\pi r^2 \rho(r) dr \\ &= 2\pi \rho_0 R_0^3 \left[\ln\left(1 + \frac{R_{\text{vir}}}{R_0}\right) + 0.5 \ln\left(1 + \frac{R_{\text{vir}}^2}{R_0^2}\right) - \arctan\left(\frac{R_{\text{vir}}}{R_0}\right) \right], \end{aligned} \quad (5)$$

where the total baryonic mass for each galaxy is estimated as $M_{\text{bar}} \simeq M_* + 1.33 M_{\text{HI}}$ (Planck Collaboration et al. 2020), the virial radius R_{vir} encloses a mean density of 200 times the critical value, R_0 and ρ_0 are free parameters denoting the core of the halo, and R_0 is related to M_{vir} as (Salucci et al. 2007),

$$\log[(R_0/\text{kpc})] = 0.66 - 0.58(\log[M_{\text{vir}}/10^{11} M_\odot]). \quad (6)$$

The halo concentration is evaluated as $c = R_{\text{vir}}/R_0$.

3. PROPERTIES OF HI-BEARING UDGs

3.1. Baryonic Tully-Fisher relation of UDGs

In the upper panel of Fig. 2, we present the baryonic Tully-Fisher relations (bTFRs) for both UDGs (depicted in magenta) and their dwarf counterparts (depicted in cyan). Consistent with previous investigations into UDG bTFRs (Mancera Piña et al. 2020; Karunakaran et al. 2020; Hu et al. 2023), our UDG sample exhibits a notable departure from the bTFRs observed in typical galaxies (McGaugh et al. 2000; Lelli et al. 2016). Specifically, the UDG bTFR is characterized by a shallower slope of $\log M_{\text{bar}} = 1.11(\pm 0.39) \log V_c + 7.46(\pm 0.73)$.

This deviation cannot be ascribed to the possible misalignment in the HI and optical inclination angles, as such misalignment would manifest as a large scatter in V_c rather than a systematic deviation. Furthermore, it cannot be ascribed to differing inclination angles between UDGs and typical dwarf samples, as the fainter objects detected are more likely to

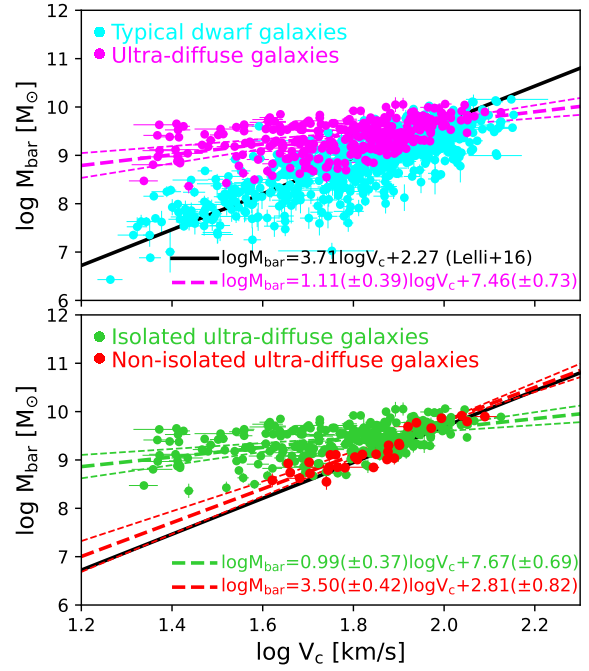


Figure 2. Upper panel: The bTFRs for HI-bearing UDGs (depicted by magenta circles) and typical dwarf counterparts (depicted by cyan circles). The bTFR observed in typical dwarfs (Lelli et al. 2016) is represented by the black line, while the magenta dashed lines correspond to the best linear fitting results (including the average and 1σ uncertainty) for our comprehensive sample of 275 UDGs in this study. **Lower panel: A comparative analysis of the bTFRs between isolated UDGs (depicted by green circles) and non-isolated UDGs (depicted by red circles).** The dashed lines also represent the optimal linear fitting outcomes for the isolated and non-isolated UDG samples, respectively.

possess larger inclinations. As depicted in Fig. 3, the bTFRs of UDGs and typical dwarfs exhibit consistent behavior across various inclination angle ranges.

Could the discrepancy be linked to limitations in telescope detection? From the perspective of HI detection, ALFALFA operates as a blind extragalactic HI survey that functions independently of galactic environments and internal properties. Given that the Arecibo beam size is approximately $3.5'$ (Haynes et al. 2018), both UDGs and typical dwarfs can be considered as “point sources” with $r_{\text{HI}} \ll 3.5'$. Consequently, UDGs and typical dwarfs should have equivalent HI mass detection limits, resulting in comparable completeness levels for both samples.

However, the detection completeness of UDGs and typical dwarfs in the SDSS dataset may differ due to the fainter surface brightness of UDGs, particularly those with low stellar masses and extremely large effective radii. Nevertheless, it is worth noting that observations and simulations consistently

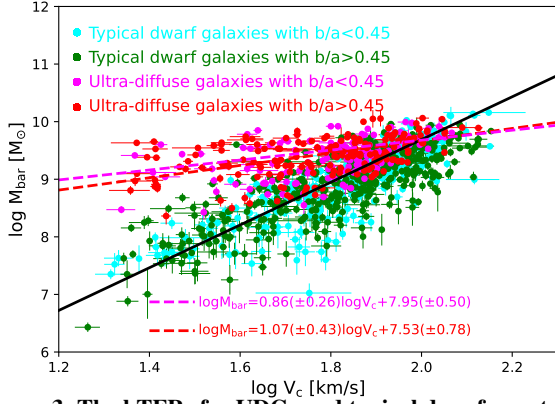


Figure 3. The bTFRs for UDGs and typical dwarf counterparts with different apparent axis ratios (i.e., different inclinations). Similar to the representation in Fig. 2, the two dashed lines correspond to the optimal linear regression results obtained for the UDG subsamples with $b/a < 0.45$ and $b/a > 0.45$, respectively.

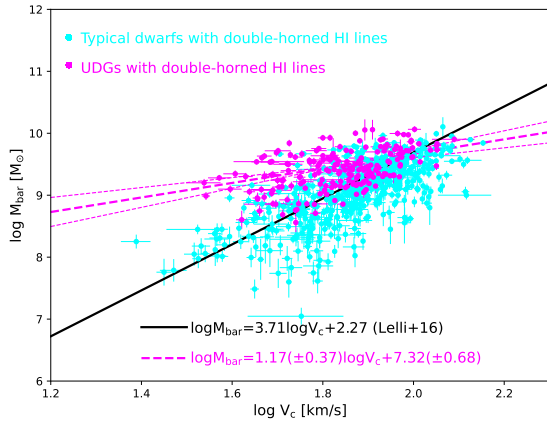


Figure 4. The bTFRs for UDGs (depicted in magenta) and typical dwarf counterparts (depicted in cyan) exhibiting double-horned HI line profiles. Similar to the representation in Fig. 2, the dashed lines correspond to the optimal linear regression results obtained for the UDG sample.

indicate that the majority (approximately 80% to 90%) of UDGs actually possess relatively small effective radii, with $R_{*,e}$ ranging from 1.5 to 3.0 kpc (Yagi et al. 2016; van der Burg et al. 2016; Rong et al. 2017; Liao et al. 2019; Di Cintio et al. 2017). Therefore, we can estimate the threshold of absolute magnitude beyond which the selection effect does not significantly impact the completeness of UDGs.

For the SDSS i -band, the 3σ (1σ) detection limit of surface brightness is approximately 25.9 (27.1) mag/arcsec² (Kniazev et al. 2004). A UDG is considered well-detected if the surface brightness at $1.5R_{*,e}$ is $\mu(1.5R_{*,e}) \lesssim 27.1$ mag/arcsec². In this case, we find that the estimates for stellar mass and effective radius of the UDG are minimally affected (e.g., introducing an error of approximately 0.14 dex in the estimate of stellar mass, which is smaller than the uncertainty in mass and can be neglected). As-

suming a Sérsic profile with an index $n = 1$ (Leisman et al. 2017; Rong et al. 2020a) for the surface brightness distribution of a UDG, we derive the mean surface brightness within the effective radius, $\langle\mu_{*}\rangle_e \sim 25.5$ mag/arcsec², from $\mu(1.5R_{*,e}) = 27.1$ mag/arcsec² (Graham & Driver 2005). Since the i -band absolute magnitude of a UDG is given by $M_i \simeq \langle\mu_{*}\rangle_e - 2.5 \log(2\pi R_{*,e}^2) - 36.57$ (Graham & Driver 2005), the magnitude threshold for a face-on UDG with $R_{*,e} = 3.0$ kpc is $M_i \sim -15.5$ mag. Therefore, for our UDG sample, comprising 98.5% of UDGs with $M_i < -15.5$ mag, the selection effect is not significant. Beyond this magnitude threshold, only 10% to 20% of UDGs have not been detected by SDSS. This implies that even if all of the undetected 10% to 20% of UDGs exhibit small M_{bar} comparable to typical dwarfs, our conclusions would remain unchanged.

Therefore, the deviation observed in the bTFR of UDGs is not attributed to the detection limits of telescopes.

Could the bTFR discrepancy of UDGs be caused by the possibility of UDGs being dominated by velocity dispersion rather than rotation? Previous work has demonstrated that HI in isolated UDGs tends to be distributed in thin discs, exhibiting regular rotation (Mancera Piña et al. 2020; Li et al. 2022). The average ratio of gas velocity dispersion to rotation velocity, denoted as $\langle\sigma/V_c\rangle$, is found to be less than 20% (Mancera Piña et al. 2020).

However, a subset of UDGs may be characterized by a prevalence of velocity dispersion rather than regular rotation. These UDGs are identified by their HI line profiles, which often manifest as a single-horned shape (ElBadry et al. 2018). Within our UDG sample, approximately 30% display these single-horned HI line profiles. To ensure the robustness of our analysis, we exclude these potentially dispersion-dominated UDGs from further investigation, and focus exclusively on UDGs with double-horned HI line profiles, which are indicative of regular rotation. As detailed in Fig. 4, when compared to typical dwarf galaxies, UDGs with double-horned HI line profiles consistently demonstrate a deviated bTFR. Therefore, the deviation observed in the bTFR of UDGs is also not attributable to the possibility that UDGs being dominated by velocity dispersion.

In conclusion, the deviation of UDG bTFR may appear to have a physical basis.

3.2. bTFR dependence on environment: UDGs are abundant in baryonic matter, not lacking in dark matter

It is worth noting that the divergent bTFR is primarily driven by the low-mass UDGs characterized by small circular velocities ($\log V_c \sim 1.4 - 1.9$), which can be theoretically explained by two plausible formation scenarios. Firstly, these UDGs may have previously been embedded in more massive halos but experienced dark matter loss due to tidal interactions (van Dokkum et al. 2018; Jing et al. 2019) or galaxy collisions (van Dokkum et al. 2022), rendering them dark matter-deficient galaxies. Alternatively, these UDGs may have originated in genuine low-mass halos but have accumulated a greater amount of baryonic matter compared to their typical dwarf counterparts.

The first scenario suggests that these low-mass UDGs are more likely to reside in high-density environments characterized by stronger tidal forces and an increased likelihood of galaxy encounters. Therefore, we investigate the environments of our UDG sample. In order to examine the environmental characteristics of each galaxy in our sample, we employ the galaxy group and cluster catalog developed by [Saulder et al. \(2016\)](#). This catalog is constructed based on the SDSS DR12 ([Alam et al. 2015](#)) and 2MASS Redshift Survey ([Huchra et al. 2012](#)), utilizing the friends-of-friends group finder algorithm. Importantly, the study conducted by [Saulder et al. \(2016\)](#) comprehensively accounts for various observational biases, such as the Malmquist bias and the ‘Fingers of God’ effect. To determine the environmental classification of galaxies, we adopt the criteria established by [Guo et al. \(2020\)](#). Specifically, galaxies are classified as non-isolated if they are located within a distance of three times the virial radius of the nearest galaxy group or cluster. Conversely, galaxies that do not satisfy this criterion are classified as isolated.

As shown in the lower panel of Fig. 2, we observe that isolated UDGs (depicted in green) exhibit a more pronounced deviation in the bTFR, while UDGs in high-density environments (depicted in red) show a bTFR closer to that of typical dwarfs. This finding supports the notion that the divergent bTFR of UDGs is more likely attributed to the excessive accumulation of baryonic matter in UDGs compared to typical dwarf counterparts, rather than a deficiency in dark matter. Therefore, the formation of UDGs cannot be ascribed to possibility (II), i.e., the elevated V_c and diminished M_* .

3.3. Constrains on UDG formation models

We also directly estimate the halo masses M_{vir} for both isolated UDGs and typical dwarf counterparts with the method described in section 2.2. Our findings reveal that the maximum halo mass in our UDG sample is approximately $2 \times 10^{11} M_\odot$, considerably less massive than the dark matter halo of an L^* galaxy, which typically reaches $10^{12} M_\odot$. This discrepancy also contradicts the failed L^* formation model proposed for UDGs ([van Dokkum et al. 2015](#)) (possibility II).

Subsequently, we conduct a direct comparison of the halo masses and baryonic fractions ($M_{\text{bar}}/M_{\text{vir}}$) between the isolated UDG and typical dwarf samples, specifically within the circular velocity range of $1.4 \lesssim \log V_c \lesssim 1.9$. As illustrated in Fig. 5, while the distributions of halo masses exhibit similarity between the two samples, the baryonic mass fractions and HI-to-stellar mass ratios (M_{HI}/M_*) of UDGs are significantly higher, indicating an excess of baryonic matter in UDGs, predominantly in the form of gas.

In empirical galaxy formation models, similar baryonic mass fractions are expected in isolated dark matter halos with comparable masses. Therefore, the higher baryonic fractions observed in UDGs suggest an ineffective outflow driven by supernovae, which fails to expel gas from halos as effectively as in typical dwarf galaxies. In other words, the heightened abundance of HI gas in UDGs cannot be adequately

attributed to significant alterations of gravitational potentials ([Mo & Mao 2004](#)) (possibility III). The gravitational potentials of the isolated UDGs and typical dwarf counterparts, characterized by the concentrations (c) of their dark matter halos, are statistically comparable, as indicated in panel (b) of Fig. 5. Consequently, the more compelling explanation for the emergence of extended stellar disk radii and reduced stellar densities in UDGs lies in their elevated specific angular momenta S_* , i.e., (possibility I).

3.4. Higher specific angular momentum in UDGs

Hence, we proceed to estimate and compare the specific angular momenta of the stellar and HI-gas components for the two samples. For a stellar disk, its specific angular momentum can be determined using equation (1)

$$S_* \propto R_{*,d} V_c. \quad (7)$$

Here the scale length is approximately $R_{*,d} \simeq R_{*,e}/1.678$ for an exponential stellar disk profile ([Graham & Driver 2005](#)). Similarly, the specific angular momentum of an HI-gas disk can be expressed as

$$S_{\text{HI}} \equiv \frac{J_{\text{HI}}}{M_{\text{HI}}} \propto R_{\text{HI},d} V_c, \quad (8)$$

where J_{HI} represents the angular momentum of the HI disk, and the scale length of the HI disk, $R_{\text{HI},d}$, can be derived by assuming a relatively thin gas disk in centrifugal balance ([Mo et al. 1998](#)), characterized by an exponential surface density profile, as

$$\Sigma_{\text{HI}}(R) = \Sigma_{\text{HI},0} \exp(-R/R_{\text{HI},d}), \quad (9)$$

where $\Sigma_{\text{HI},0}$ represents the central surface density of the HI disk. The total HI mass M_{HI} is related to the scale length as

$$M_{\text{HI}} = 2\pi \Sigma_{\text{HI},0} R_{\text{HI},d}^2. \quad (10)$$

Furthermore, by definition, at r_{HI} , we have

$$\Sigma_{\text{HI},0} \exp(-r_{\text{HI}}/R_{\text{HI},d}) = 1 M_\odot \text{pc}^{-2}. \quad (11)$$

Using equations (10) and (11), we can calculate the value of $R_{\text{HI},d}$ for each galaxy in our sample.

Therefore, by utilizing equations (7) and (8), the comparison of the stellar and HI specific angular momenta between the UDG and dwarf counterpart samples can be simplified as a comparison of the observable quantities $R_{*,d} V_c$ and $R_{\text{HI},d} V_c$, respectively. As illustrated in panels (e) and (f) of Fig. 5, the average specific angular momenta (or spins) of UDG stellar and HI-gas disks are approximately 0.4 dex higher than those of the dwarf counterparts on a logarithmic scale.

We further present the comparative outcomes for the resilient subsets of solitary UDGs and typical dwarfs possessing double-horned HI profiles. As illustrated in Fig. 6, the findings align with those of the entire dataset.

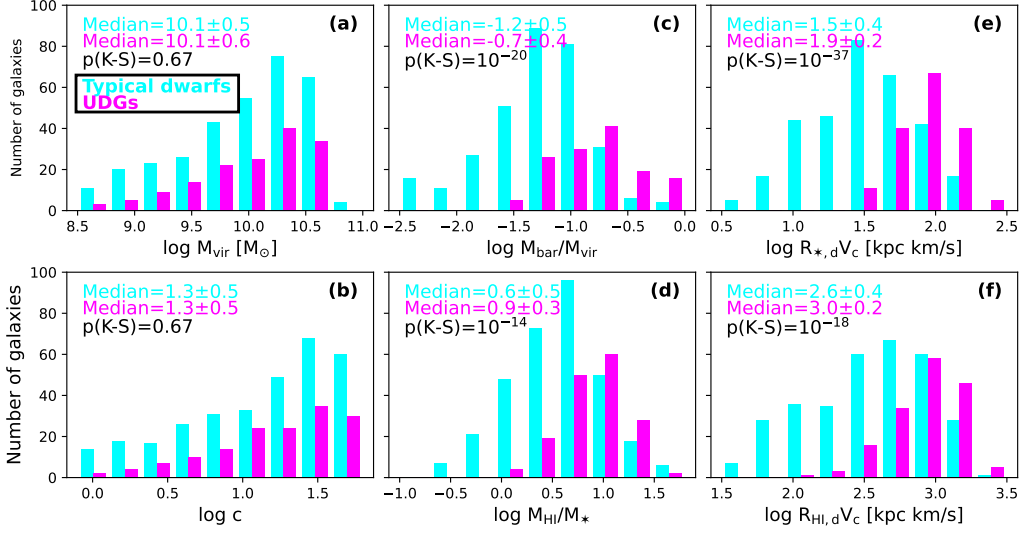


Figure 5. The comparative analysis between isolated UDGs (depicted in magenta) and typical dwarf counterparts (depicted in cyan). Panels a to f present histograms displaying the distributions of halo masses, halo concentrations, baryonic mass fractions, HI-to-stellar mass ratios, as well as $R_{*,d}V_c$ and $R_{HI,d}V_c$ (which can be considered as proxies for their stellar and HI specific angular momenta), for UDGs and typical dwarfs, respectively. The logarithmic scale is employed to represent the median value of each property, and the Kolmogorov-Smirnov test p -value is provided to assess the disparity in property distributions between the two galaxy samples, as indicated in the corresponding panel.

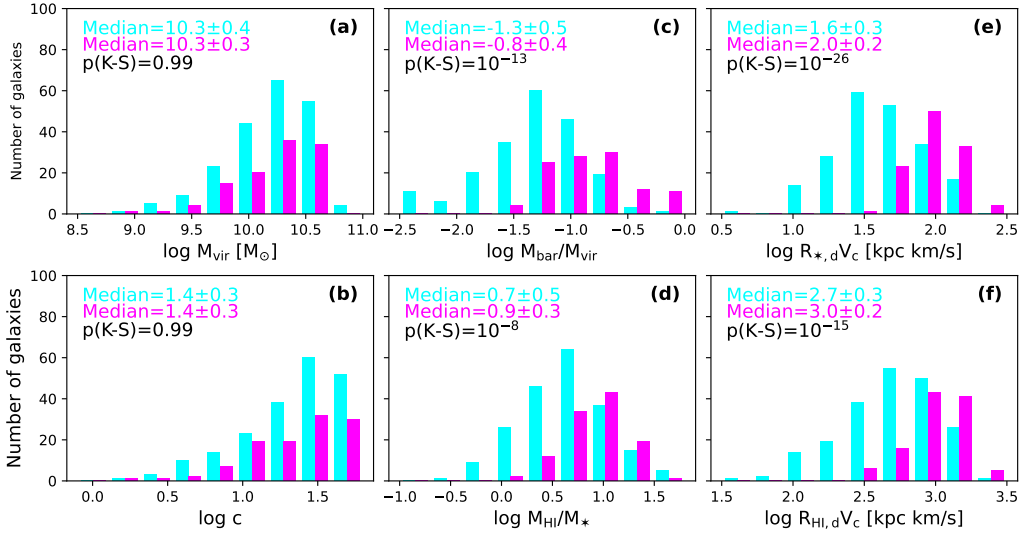


Figure 6. A comparative analysis between isolated UDGs (represented in magenta) and typical dwarf counterparts (represented in cyan) exhibiting double-horned HI line profiles. The selected samples encompass the same range of circular velocities with $1.5 \lesssim \log V_c \lesssim 1.9$. Each panel within this study is analogous to the corresponding one depicted in Fig. 5.

4. DISCUSSION AND SUMMARY

In this investigation, we initially classified the existing UDG formation models into three possibilities, (I) higher S_* , (II) elevated V_c and diminished M_* , and (III) a change in gravitational potential. Subsequently, we selected the sample of HI-bearing UDGs in observational data and compared their properties with those of typical dwarf counterparts. Our analysis ultimately dismisses the second and third forma-

tion possibilities, attributing the origin of HI-bearing UDGs to their elevated specific angular momentum, predominantly aligning with possibility (I). Nonetheless, we are unable to definitively discern whether the higher S_* of UDGs arises from a higher halo spin or a greater spin of the accreted gas, albeit with comparable halo spin to typical dwarfs.

Although this formation model is not novel and has been supported by cosmological hydrodynamical simulations (Be-

navides et al. 2023), as well as semi-analytic galaxy formation models implemented on N -body simulations (Rong et al. 2017; Amorisco & Loeb 2016), and also been proposed by observational UDG studies (e.g., Mancera Piña et al. 2020), our study, for the first time, provides statistical observational evidence to validate this formation mechanism and reject other formation possibilities.

As mentioned in section 1, several observational studies on the kinematics of UDGs do not support the higher S_* compared to typical dwarfs. However, it is important to note that these observations primarily pertain to UDGs in high-density environments, which may have undergone tidal heating, possibly leading to a reduction in their S_* .

The discovery of higher S_* and S_{HI} in UDGs provides a comprehensive understanding of UDG formation. We propose that UDGs emerged within dark matter halos possessing masses akin to those of dwarf galaxies. Nevertheless, in contrast to typical dwarfs, the halos of UDGs exhibited augmented rotational velocities or experienced the acquisition of faster rotating circumgalactic medium from their surroundings. As a consequence, UDGs harbor highly-spinning HI gas. This highly-spinning gas demonstrates greater resilience against angular momentum loss, impeding its descent towards the galactic core and subsequent condensation and cooling necessary for providing the cold (< 100 K) fuel essential for star formation in the central regions of the halo (Peng & Renzini 2020). The inflow of gas into the central region of a UDG is therefore gradual and continuous, ensuring a sustained supply. This gradual inflow precludes the instantaneous ignition of a substantial burst of star formation or the triggering of supernova explosions en masse, thus preventing the expulsion of a large amount of HI gas from UDGs beyond the confines of the dark matter halo. This intricate mechanism ultimately culminates in the accumulation

of excessive HI masses, reduced star formation efficiencies, diminished stellar densities, and the expansion of stellar disk radii observed in UDGs.

Many observational and theoretical studies on UDGs concur that these low-surface-brightness objects tend to have lower star formation rates and a more extended star formation history (e.g., Rong et al. 2020a; Trujillo et al. 2017; Di Cintio et al. 2017), which conversely support the higher S_{HI} in UDGs based on the aforementioned scenario. Conversely, the protracted star formation history may also account for the abundant presence of globular clusters in numerous UDGs (Forbes et al. 2020). If star formation predominantly occurred in the early Universe, the constituent globular clusters may have undergone substantial mass loss due to stellar evolution (Lamers et al. 2010; Carretta et al. 2010; Decressin et al. 2010), rendering them faint and challenging to detect. In contrast, an extended star formation process naturally results in a broad range of ages among member globular clusters, potentially preserving a larger number of detectable globular clusters at redshift $z \sim 0$.

1 Y.R. acknowledges supports from the NSFC grant
2 12273037, and the CAS Pioneer Hundred Talents Program
3 (Category B), as well as the USTC Research Funds of the
4 Double First-Class Initiative. W.D. is supported by the Youth
5 Innovation Promotion Association, Chinese Academy of Sci-
6 ences No. 2020057. Q.G. is supported by the National SKA
7 Program of China No. 2022SKA0110201, the CAS Project
8 for Young Scientists in Basic Research Grant No. YSBR-
9 062, and the European Union’s Horizon 2020 Research and
10 Innovation Programme under the Marie Skłodowska-Curie
11 grant agreement No. 101086388. H.Y.W. is supported by
12 CAS Project for Young Scientists in Basic Research, Grant
13 No. YSBR-062, and the NSFC grant 12192224. H.X.Z. ac-
14 knowledges support from the NSFC grant 11421303.

REFERENCES

- Alam, M. P., et al. 2015, ApJS, 219, 12
- Amorisco, N. C. & Loeb, A. 2016, MNRAS, 459, L51
- Bell, E. F., McIntosh, D. H., Katz, N., Weinberg, M. D. 2003, ApJS, 149, 289
- Benavides, J. A., Sales, L. V., Abadi, M. G., Marinacci, F., Vogelsberger, M., Hernquist, L. 2023, MNRAS, 522, 1033
- Bertin, E. & Arnouts, S. 1996, A&AS, 117, 393
- Burkert, A. 1995, ApJL, 447, L25
- Cardona-Barrero, S., Di Cintio, A., Brook, C. B. A., Ruiz-Lara, T., Beasley, M. A., Falcón-Barroso, J., Macciò, A. V. 2020, MNRAS, 497, 4282
- Carleton, T., Errani, R., Cooper, M., Kaplinghat, M., Penarrubia, J., Guo, Y. 2019, MNRAS, 485, 382
- Carretta, E., Bragaglia, A., Gratton, R. G., Recio-Blanco, A., Lucatello, S., D’Orazi, V., Cassisi, S. 2010, A&A, 516, A55
- Chan, T. K. et al. 2018, MNRAS, 478, 906
- Chilingarian, I. V., Afanasiev, A. V., Grishin, K. A., Fabricant, D., Moran, S. 2019, ApJ, 884, 79
- Decressin, T., Baumgardt, H., Charbonnel, C., Kroupa, P. 2010, A&A, 516, A73
- Di Cintio, A., Brook, C. B., Dutton, A. A., Maccio, A. V., Obreja, A., Dekel, A. 2017, MNRAS, 466, L1
- Disney, M. J. 1976, Nature, 263, 573
- Du, W., Wu, H., Lam, M. I., Zhu, Y., Lei, F., Zhou, Z. 2015, AJ, 149, 199
- Duc, P.-A., Bournaud, F. 2008, ApJ, 673, 787
- Durbala, A., Finn, R. A., Crone Odekon, M., Haynes, M. P., Koopmann, R. A., O’Donoghue, A. A. 2020, AJ, 160, 271
- ElBadry, K. et al. 2018, MNRAS, 473, 1930
- Forbes, D. A., Alabi, A., Romanowsky, A. J., Brodie, J. P., Arimoto, N. 2020, MNRAS, 492, 4874
- Gault, L. et al. 2021, AJ, 909, 19

- Giovanelli, R. *et al.* 2005, *AJ*, 130, 6
- Giovanelli, R. *et al.* 1997, *AJ*, 113, 22
- Graham, A. W. & Driver, S. P. 2005, *PASA*, 22, 118
- Grishin, K. A., Chilingarian, I. V., Afanasiev, A. V., Fabricant, D., Katkov, I. Y., Moran, S., Yagi, M. 2021, *NewA*, 5, 1308
- Guo, Q., *et al.* 2011, *MNRAS*, 413, 101
- Guo, Q. *et al.* 2020, *NewA*, 4, 246
- Haynes, M. P. *et al.* 2018, *ApJ*, 861, 49
- Herrmann, K. A., Hunter, D. A., Zhang, H.-X., Elmegreen, B. G. 2016, *Science*, 152, 177
- Hu, H.-J., Guo, Q., Zheng, Z., Yang, H., Tsai, C.-W., Zhang, H.-X., Zhang, Z.-Y. 2023, *ApJL*, 947, L9
- Huchra, J. P. *et al.* 2012, *ApJS*, 199, 26
- Hunter, D. A., *et al.* 2012, *AJ*, 144, 134
- Janowiecki, S., *et al.* 2015, *ApJ*, 801, 96
- Jiang, F., Dekel, A., Freundlich, J., Romanowsky, A. J., Dutton, A. A., Maccio, A. V., Di Cintio, A. 2019, *MNRAS*, 487, 5272
- Jing, Y., Wang, C., Li, R., Liao, S., Wang, J., Guo, Q., Gao, L. 2019, *MNRAS*, 488, 3298
- Karunakaran, A., Spekkens, K., Zaritsky, D., Donnerstein, R. L., Kadowaki, J., Dey, A. 2020, *ApJ*, 902, 39
- Kniazev, A. Y., Grebel, E. K., Pustilnik, S. A., Pramskij, A. G., Kniazeva, T. F. 2004, *AJ*, 127, 704
- Kong, D., Kaplinghat, M., Yu, H.-B., Fraternali, F., Mancera Piña, P. E. 2022, *ApJ*, 936, 166
- Kroupa, P. 2002, *Science*, 295, 82
- Lamers, H. J. G. L. M., Baumgardt, H., Gieles, M. 2010, *MNRAS*, 409, 305
- Leisman, L., *et al.* 2017, *ApJ*, 842, 133
- Lelli, F., McGaugh, S. S., Schombert, J. M. 2016, *ApJL*, 816, L14
- Li, X., Shi, Y., Zhang, Z.-Y., Chen, J., Yu, X., Wang, J., Gu, Q., Li, S. 2022, *MNRAS*, 516, 4220
- Liao, S. *et al.* 2019, *MNRAS*, 490, 5182
- Mancera Piña, P. E., Aguerra, J. A. L., Peletier, R. F., Venhola, A., Trager, S., Choque Challapa, N. 2019, *MNRAS*, 485, 1036
- Mancera Piña, P. E. *et al.* 2020, *MNRAS*, 495, 3636
- McGaugh, S. S., Schombert, J. M., Bothun, G. D., de Blok, W. J. G. 2000, *ApJL*, 533, L99
- Mo, H. J. & Mao, S. 2004, *MNRAS*, 353, 829
- Mo, H. J., Mao, S. D. & White, S. D. M. 1998, *MNRAS*, 295, 319
- Peng, E., Lim, S. 2016, *ApJL*, 822, L31
- Peng, Y.-J. & Renzini, A. 2020, *MNRAS*, 491, L51
- Planck Collaboration *et al.* 2020, *A&A*, 641, A6
- Posti, L., Pezzulli, G., Fraternali, F., Di Teodoro, E. M. 2018, *MNRAS*, 475, 232
- Román, J., Jones, M. G., Montes, M., Verdes-Montenegro, L., Garrido, J., Sánchez, S. 2021, *A&A*, 649L, 14
- Rong, Y., Guo, Q., Gao, L., Liao, S., Xie, L., Puzia, T. H., Sun, S., Pan, J. 2017, *MNRAS*, 470, 4231
- Rong, Y., Zhu, K., Johnston, E. J., Zhang, H.-X., Cao, T., Puzia, T. H., Galaz, G. 2020a, *ApJL*, 899, L12
- Rong, Y. *et al.* 2020b, *ApJ*, 899, 78
- Salucci, P. *et al.* 2007, *MNRAS*, 378, 41
- Saulder, C., van Kampen, E., Chilingarian, I. V., Mikske, S., Zeilinger, W. W. 2016, *A&A*, 596, A14
- Shi, Y., Zhang, Z.-Y., Wang, J., Chen, J., Gu, Q., Yu, X., Li, S. 2021, *ApJ*, 909, 20
- Sifón, C., van der Burg, R. F. J., Hoekstra, H., Muzzin, A., Herbonnet, R. 2018, *MNRAS*, 473, 3747
- Taylor, E. N. *et al.* 2011, *MNRAS*, 418, 1587
- Trujillo, I., Roman, J., Filho, M., Sánchez Almeida, J. 2017, *ApJ*, 836, 191
- Tully, R. B., Rizzi, L., Shaya, E. J., Courtois, H. M., Makarov, D. I., Jacobs, B. A. 2009, *AJ*, 138, 323
- van der Burg, R. F. J., Muzzin, A., Hoekstra, H. 2016, *A&A*, 590, A20
- van Dokkum, P. G., *et al.* 2015, *ApJL*, 798, L45
- van Dokkum, P. G. *et al.* 2016, *ApJL*, 828, L6
- van Dokkum, P. *et al.* 2018, *Nature*, 555, 629
- van Dokkum, P. *et al.* 2019a, *ApJL*, 874, L5
- van Dokkum, P. *et al.* 2019b, *ApJ*, 880, 91
- van Dokkum, P. *et al.* 2022, *Nature*, 605, 435
- Wang, J., Koribalski, B. S., Serra, P., van der Hulst, T., Roychowdhury, S., Kamphuis, P., Chengalur, J. N. 2016, *MNRAS*, 460, 2143
- Wright, A. C., Tremmel, M., Brooks, A. M., Munshi, F., Nagai, D., Sharma, R. S., Quinn, T. R. 2021, *MNRAS*, 502, 5370
- Yagi, M., Koda, J., Komiyama, Y., Yamanoi, H. 2016, *ApJS*, 225, 11
- Yozin, C. & Bekki, K. 2015, *MNRAS*, 452, 937